Wigner molecules and charged excitons in near-field magnetophotoluminescence spectra of self-organized InP/GaInP quantum dots

A. M. Mintairov,[1,2,*] J. Kapaldo,[1] J. L. Merz,[1] A. S. Vlasov,[2] and S. A. Blundell[3]
[1]*University of Notre Dame, Notre Dame, Indiana 46556, USA*
[2]*Ioffe Physical-Technical Institute of the Russian Academy of Sciences, Saint Petersburg, 194021, Russia*
[3]*University Grenoble Alpes, INAC-SyMMES, F-38000 Grenoble, France and CEA, INAC-SyMMES, F-38000 Grenoble, France*

(Received 31 August 2016; revised manuscript received 22 December 2016; published 31 March 2017)

We used high-spatial-resolution, low-temperature near-field scanning optical microscopy (NSOM) operating at magnetic fields $B = 0$–10 T to study the effects of Wigner localization (WL) on emission spectra of single self-organized InP/GaInP quantum dots (QDs) and investigate the stability of singly (trion) and doubly (tetron) charged exciton complexes in the weak quantum confinement regime. Using NSOM measurements together with configuration interaction calculations, we identify the dots having different electron population N(N = 1–12), quantum confinement ($\hbar\omega_0 = 0.6$–8 meV) and size $D(D = 70$–170 nm). For N = 2, we observed a magnetic-field-induced molecular-droplet transition, accompanied by the decomposition of the tetron into a Wigner molecule complex (WMC), and the activation of rotovibronic structure. For N = 1, unusually strong vibronic structure resulting from a trion-type WMC was observed. We have shown that magnetic-field-induced shifts of this structure allow measurement of single particle Fock-Darwin levels and angular momentum transitions of the WMC. In addition, we demonstrated the use of NSOM imaging to probe the charge density distribution and observed anomalous dependence of the image size on the quantum confinement, implying a pairing of electrons or formation of whispering gallery modes in the QD. We demonstrated that InP/GaInP QDs, provide a Wigner-Seitz radius (r_s) up to 13, and that the measurements of NSOM magneto-optical spectroscopy using these dots makes it possible to study effects arising from strong Coulomb interaction of a few confined electrons (holes).

DOI: 10.1103/PhysRevB.95.115442

I. INTRODUCTION

The Coulomb interaction plays a key role in the optical processes in semiconductors and leads to formation of a bound electron-hole (e-h) complex, known as an exciton, which is a solid state analog of the hydrogen atom [1–2]. Charged excitonic complexes (ECs) xe-h and e-xh, were x is an integer, were also predicted to exist in systems having a low density of free carriers in the conduction or valence band [3]. The Coulomb interaction is increased in quantum confined systems, and ECs having charge up to $\pm 6e$ were observed in the emission spectra of electrostatically controlled self-organized semiconductor quantum dots (QDs) [4], providing a strong confinement regime with a density of electron (hole) droplets $>10^{11}$ cm^{-2}. On the other hand, no charged ECs are observed in the optical spectra of modulation-doped quantum wells (QWs) at densities of two-dimensional (2D) electron and hole gases $>10^{11}$ cm^{-2}, and only singly charged excitons (trions [TR]) are observed at lower densities [5–10]. It was also shown [11,12] that negatively charged trions (TR$^-$) in modulation doped QWs have a very small binding energy $\sim$0.5 meV and are formed by single electrons localized by potential fluctuations induced by remote donors. Furthermore, it was found [13,14] that positively charged trions (TR$^+$) have a smaller binding energy than TR$^-$ and that the binding energy of both increases strongly with decrease of QW thickness. These experiments indicate the critical role of quantum confinement for the stability of multicharged ECs and raise the question of their existence as free quasiparticles.

The stability of ECs can be probed using emission spectra of systems having weak quantum confinement, for which ECs behave as classical particles and which can be identified by a specific dependence of their emission energy on a magnetic field and an appearance of Stokes (shake up) emission components [15,16]. In particular, a negatively charged EC is predicted to have paramagnetic response.

In weak quantum confined systems, the energy of the Coulomb interaction between the electrons may exceed their kinetic energy, which induces a molecular regime, i.e. a spatial ordering and partial localization of electrons, predicted by Wigner in 1934 [17] and known as Wigner localization (WL). For quasi-2D dots, the ratio of Coulomb-to-kinetic energy and the degree of WL is characterized by the dimensionless density parameter (Wigner-Seitz radius) $r_s = 1/[a_B{}^*(\pi \cdot n)^{0.5}]$, where $a_B{}^*$ is the effective Bohr radius [18] and n is the average electron density in the plane of the dot. It can also be expressed via the parabolic (harmonic) potential frequency ω_0 via $r_s = \omega_0^{-0.5}$, where ω_0 is expressed in units of effective Hartrees, Ha* [19]. In general, depending on the stability of ECs and r_s, a formation of different photoexcited EC-molecular complexes can be expected. Also, WL is enhanced in a perpendicular magnetic field [20], which can modify the formation of these complexes. A specific case of TR formation in a two-electron (2e) Wigner molecule (WM) at zero magnetic field was analyzed in Ref. [16]. The predicted emission spectrum contains several Stokes components, which can be related to the center-of-mass (c.m.) and the relative rotovibration motion of two electrons [21–23]. Thus, if an EC

*amintair@nd.edu

is unstable and decomposes into a photoexcited WM complex, further denoted as WMC, the emission of specific Stokes components is expected to appear, which can be identified using photoluminescence (PL) spectroscopy. However, so far, PL experiments on weak quantum confined systems include only vertical nanofabricated GaAs/AlGaAs QDs [24] having electron population $N \geqslant 4$, relatively strong confinement ($\hbar\omega_0 = 3.35$ meV), and weak WL ($r_s = 1.71$) [25], which does not allow identification of EC versus WMC emission.

In this paper, we have used a material system allowing for weak quantum confinement, providing much stronger WL effects. This system consists of large (∼150 nm) self-organized InP/GaInP QDs grown by metal-organic chemical vapor deposition. The dots having electron population N up to 12, quantum confinement down to $\hbar\omega_0 = 0.6$ meV and size D up to 170 nm were studied using high-spatial-resolution near-field (NF) magneto-PL spectroscopy and imaging. We used two electron dots to observe a molecular-droplet transition induced by a magnetic field and identify the emission spectra of 2e-WM. In dots having a single electron (hole), we observed unusual "vibronic" structure manifesting decomposition of a TR and formation of a 2e-h (2h-e) WMC. We demonstrate that the shift of this structure in a magnetic field allows the direct measure of single particle Fock-Darwin (FD) levels and angular momentum transitions of the WMC. Our results give evidence of the decomposition of ECs at the onset of WL for $r_s \sim 2.5$ and demonstrate that free ECs do not exist. In addition, using NF PL imaging and configuration interaction calculations of charge density (CD), we observed anomalous dependence of the image size on the quantum confinement, implying the formation of a whispering gallery mode (WGM) or pairing of electrons. We show that InP/GaInP QDs, providing a Wigner-Seitz radius up to 13, allow for the study of WL, using NSOM magneto-optical spectroscopy.

II. SAMPLE GROWTH AND EXPERIMENTAL DETAILS

The sample was grown on a GaAs substrate by metal-organic chemical vapor deposition in a horizontal AIX200/4 reactor under 100 mbar pressure at temperature 725 °C. The dots are formed by deposition of seven monolayers of InP on $Ga_{0.52}In_{0.48}P$ latticed matched to the GaAs and capped by a 60 nm thick $Ga_{0.52}In_{0.48}P$ layer. We used a GaAs substrate misoriented by 2° towards the [110] direction. The results of detailed structural, chemical, and optical characterization of this QD structure using transmission electron microscopy (TEM) and PL measurements together with the results of a self-consistent calculation of exciton transitions using an effective mass, mean field theory with an isotropic elasticity model, calculations of shell splitting using a mean field Hartree-Fock approach, and calculations of electron density distributions using a configuration interaction approach, were all reported in Ref. [26].

Single dot magneto-PL was measured using a cryo-NF scanning optical microscope (NSOM) operating at 10 K and magnetic fields up to 10 T. We used tapered fiber probes coated by Al, having aperture size ∼100 nm in collection-illumination mode, as described in Ref. [27]. The spectra were excited by the 514.5 nm Ar laser line and measured using a charge-coupled device (CCD; multichannel) or an avalanche photodiode (APD) (single channel) detector together with a 280 mm focal length monochromator. The excitation power measured before fiber coupler was ∼5 μW, which provided power density ∼0.5 W/cm^2. The spectral resolution of the system is 0.2–0.4 meV.

For Lorenz contour deconvolution, we used a multipeak fitting procedure from Origin 8.0 graphic software.

The images at the selected wavelengths were generated using the CCD spectra taken in a square grid having mesh 100 and 50 nm or directly measured using the APD detection during topography scanning. We plotted the experimental data using a contour plot option of Origin 8.0 and division of the intensity data into 20 levels. The images taken during topography scanning, having 3 nm steps, were smoothed by averaging the intensity data over 20 nm steps.

III. STRUCTURAL AND EMISSION PROPERTIES OF INP/GAINP QDs

The TEM measurements have shown the size distribution peaked at 140 nm having a full width half maxima (FWHM) 80 nm. The dots reveal small elongation and asymmetry, which in most cases can be described as a combination of ∼5% elliptical distortion ($D_\parallel / D_\perp = 1.05$) and 10% change of $R_\perp$ (see Fig. 5 in Appendix). The dots have a lens-type shape and bimodal height distribution peaked at ∼5 and ∼20 nm, which we assign to A- and B-type dots, respectively. The dots have emission energy near 1.79 and 1.71 eV for A and B dots, respectively, which corresponds to Ga composition of 15%, which follows from TEM measurements and the exciton transition calculations assuming uniform Ga distribution. Calculations show type-I (direct) exciton transitions induced by Coulomb interaction and involving a weakly localized heavy hole.

Preferential electron accumulation in the B dots, resulting from unintentional doping of the upper GaInP layer, was revealed using measurements of the circular polarization degree of the ensemble emission spectra.

In our previous studies (see Refs. [26,27]), we measured the PL spectra of more than 20 single dots of type B emitting in the range 1.66–1.76 eV, which results from the difference of Ga content ranging from 7 to 20%. The single dot spectra revealed a rich multipeak structure resulting from electron occupation and consisting of a main peak and few Stokes/anti-Stokes peaks having energy $\Delta E = \pm(1\text{–}10)$ meV. The FWHM of the peaks is ∼0.5 meV for $|\Delta E| < 3$ meV and ∼3 meV for larger splitting. Up to four anti-Stokes and six Stokes peaks were observed for different dots. The spectra of selected dots having $N = 1\text{–}12$ are presented in the Appendix.

Accounting for the fact that our dots are doped by electrons and have large size together with noncircular shape, we assign anti-Stokes components to emission from occupied electronic shells (s, p, d, . . .) and Stokes components to rotovibrational modes of c.m. and relative electron motion. This agrees well with the prediction of emission spectra of a 2e molecule from Ref. [16]. Thus, we can estimate the number of electrons (using the number of electrons accepted by a particular shell) from the number of observed anti-Stokes peaks and the size of the dots from their energy $\Delta E \approx \hbar\omega_0$. From configuration-averaged Hartree-Fock calculations, we estimated the dot size up to

180 nm for $\hbar\omega_0 = 1.5$ meV, which is in the upper range of the dot size distribution. For this size and confinement, the calculations of the electron density distribution using a configuration-interaction approach show clear WL effects resulting in a dimer having length ~60 nm for N = 2 and a ring having size ~100 nm for N = 6 (see Fig. 6 in the Appendix). Our preliminary measurements, presented in the Appendix, have shown that the size of the NF emission intensity image of dots having different N and $\hbar\omega_0$ is close to the calculated size of the electron density, but with some exception. This implies a uniform potential distribution over the physical size of the dot (i.e., no Ga clustering) and a true weak quantum confinement regime.

Thus, our dots serve as an appropriate nanolaboratory to study the stability of charged exciton complexes, and we can select the dot having one electron as the dot which does not have anti-Stokes peaks, and the dot having two electrons as the dot having only one anti-Stokes peak in the emission spectra. For N = 2 (electronic helium), molecular states were calculated in detail for a wide range of density parameter r_s (see Refs. [21–23]).

We should point out that the emission spectra of electrons in a QD having weak quantum confinement and size 100–200 nm observed is quite different from the spectra of much smaller dots having size 10–20 nm providing strong quantum confinement [4]. In the strong quantum confinement dots, the spectra of electronic droplets result from electron exchange and promotion-demotion processes in the final state of the emission process [28]. This mechanism is governed by the exchange interaction, which decreases as the dot size increases and thus makes a weak contribution in our dots. Also, in the weaker confinement conditions the noninteracting harmonic-oscillator shell structure is distorted and becomes less well defined (see Ref. [26]), which can be expected to qualitatively change the appearance of the emission spectrum. At weak confinement, it is necessary to account for WL effects and the activation of rotovibrational modes.

Below, we present the results of the measurements of two dots having N = 2, denoted as QD2 and QD10, and three dots having N = 1, denoted as QD1, QD4, and QD9. Our magneto-PL results gave strong evidence that QD1 contains a single hole instead of an electron.

IV. MOLECULAR STATE FOR N = 2

A. Molecular-droplet transition

In Fig. 1, we show spectra of QD2 together with their Lorentz contour decomposition in magnetic fields 0, 1, 2, . . . 10 T. At zero field, a single band, denoted as *A*, having maximum at 1.7503 eV and $\gamma = 2$ meV, is observed. This band partially overlaps with the high energy tail of neighboring dot QD1 emitted at lower energy. With increasing magnetic field, the *A* band shifts to lower energy, i.e. shows paramagnetic response. At $B = 3$ T, a low-energy (Stokes) shoulder appears, and at $B = 10$ T, it is clearly resolved as a separate band *B*, shifted from the *A* band by −1.4 meV and having $\gamma =$ 1.1 meV. Also, at 10 T, a weak high energy, anti-Stokes band *C* shifted +2.2 meV appears.

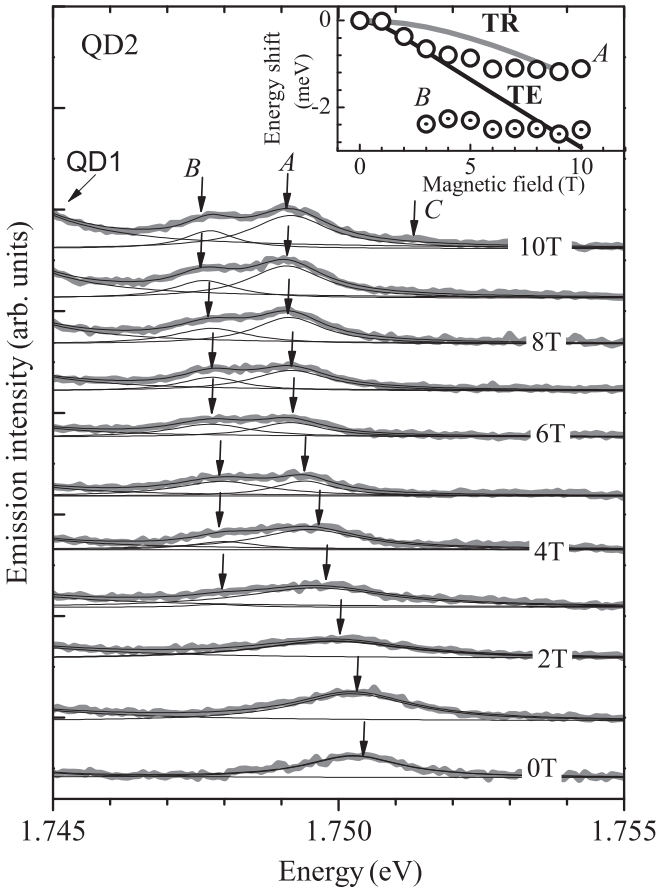

FIG. 1. NF spectra of the InP/GaInP QD labeled QD2 at magnetic field $B = 0,1,2,\ldots,10$ T. Arrows show positions of peaks *A*, *B*, and *C*. Insert shows the energy shift of *A* and *B* peaks (circles) and calculations (curves) of these shifts of singly and doubly charged excitons, i.e. TR and TE, respectively, versus magnetic field.

We should point out that the observed paramagnetic behavior in our large dots is related to weak quantum confinement, in contrast to that observed in small QDs under the conditions of electron delocalization [29,30] or mixing of the hole states [31,32].

We analyzed the magnetic field shift of the band *A* using single-particle FD theory [33] and assuming weak confinement. Using the approach of Ref. [15], the FD emission spectrum of the EC at zero field in the low temperature limit ($\hbar\omega_x \gg kT$, where k is the Boltzmann constant) is

$$E_x = E_{0x} + \hbar\omega_x - \hbar\omega_0(2N + |M| + 1), \qquad (1)$$

where E_{0x} is the "free" 2D EC energy, $\omega_x = [(xm_e^*\omega_0^2 + m_h^*\omega_{0h}^2)/(xm_e^* + m_h^*)]^{0.5}$,$\omega_0(\omega_{0h})$ and $m_e^*(m_h^*)$ are the parabolic frequency and effective mass of electrons (holes), respectively, and $N(M)$ is a radial (azimuthal) quantum number of the electron droplet left in its final state. The value of effective mass of the heavy hole for our InP/GaInP QDs is $m_h^* = 0.6$ [34]. Due to selection rules $M = 0$. Since $\omega_x \neq \omega_0$, weak Stokes components related to transitions from a (0,0) ground state of EC_x to (0,*N*) states of an electron droplet become active. These components, however,

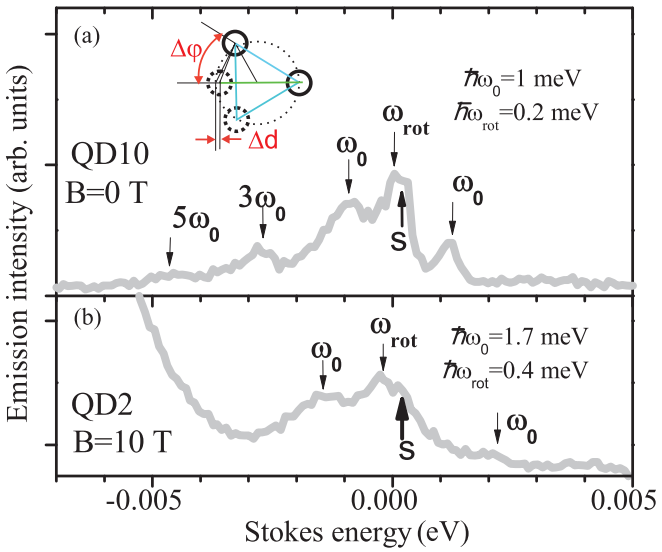

FIG. 2. NF PL spectra of (a) InP/GaInP QD10 and (b) QD2, representing two-electron WMs at (a) $B = 0$ and (b) $B = 10$ T magnetic field. Inset shows electron positions in a 3e-WMC versus a 2e-WM.

can hardly be resolved in our spectra due to the contribution of QD1.

A magnetic-field-induced shift of the main transition $\langle 0|0\rangle$ can be approximated from Eq. (1) by replacing ω_x with $\omega_x(B) = [\omega_x^2 + (\omega_{cx}/4)^2]^{0.5}$, where $\omega_{cx} = xeB/m_x^*$ is the cyclotron frequency of the EC. For a negatively charged EC $\omega_x \ll \omega_{x-1}$ (since $m_e^* \ll m_h^*$) and $\Delta E_x(B) = E_x(B) - E_{0x} < 0$; i.e. the $< 0|0 >$-transition has a paramagnetic shift. We calculated the shift of TR and 2e-EC-tetron (TE), using the above formula and plotted the results in the insert in Fig. 1. One can see good agreement between the experimental data for the A peak and the calculated TE shift for B up to 3 T, thus confirming its EC^- origin. For higher B, the shift becomes smaller than the calculated curve and saturates for $B = 6$ T at a value -1.1 meV. This indicates a transition from a 2e-droplet to a 2e-WM, which manifests itself by the appearance of B and C bands, and implies a decomposition of the TE, i.e. formation of a 3e-h WMC.

B. Rotovibrational states in emission spectra

In Fig. 2, we compare the spectrum of QD2 at $B = 10$ T and the $B = 0$ spectrum of dot QD10, which was previously assigned to be a 2e-WM at zero field [27]. The horizontal axis in the spectra represents Stokes energy. It is seen that the spectra of both dots have similar structure, differing mainly by the separation of the components, their width and number. For QD10, the $\langle 0|0\rangle$-peak has three times smaller width ($\sim$0.6 meV), nearly two times smaller separation between the components ($\sim$1 meV) and two additional Stokes peaks compared with those of QD2. The overall features of the spectra in Fig. 2 (i.e., the Stokes structure and anti-Stokes peak) correspond to the emission structure expected for a 2e-WM, as suggested in Ref. [16].

The excitation energies of a 2e-WM can be written as (see Ref. [23])

$$\delta E = Rm^2 + Tn + (2N + |M|)\hbar\omega_0, \qquad (2)$$

where m and n are quantum numbers related to rotational and stretching modes of the relative motion, M and N are azimuthal and radial quantum numbers, respectively, of the c.m. motion, $R \approx 0.37\hbar\omega_0$, and $T \approx 1.75\hbar\omega_0$. Each state in a 2e-WM has a total spin $S = [1 - (-1)^m]/2$, i.e. either $S = 0$ or $S = 1$. The formation of a 3e-h-WMC in the photoexcited state induces mainly rotational and azimuthal degrees of freedom as shown in an inset in Fig. 2. It is seen that, after the recombination of one electron with the hole, the relaxation of the two remaining electrons results in a change of the angle of the mutual electron arrangement by $\Delta\varphi = 30°$. At the same time, the distortion of bond length Δd is small ($\sim$5%), which suppresses activation of radial and stretching modes. Thus, rotational and c.m. modes having $m = 1$ and odd M dominate in the emission spectra. Thus, the $\langle 0|0\rangle$ peak shifts on R, and the Stokes peaks can be attributed to $\langle 0|1\rangle$, $\langle 0|3\rangle$, and $\langle 0|5\rangle$ transitions, denoted as ω_0, $3\omega_0$, and $5\omega_0$. In the spectra in Fig. 2, we measured $\hbar\omega_0 =$ 1.0 and 1.7 meV, and $R = 0.2$ and 0.4 meV, for QD10 and QD2, respectively. Thus, we get $r_s = 3.6$ for QD10 at $B = 0$ and $r_s = 2.8$ for QD2 at $B = 10$ T, respectively.

We should point out that paramagnetic response was observed in QWs for the "ensemble" TR PL line at fields below 2 T, and diamagnetic response was observed at higher fields (cf. Refs. [4,35]); in light of the results reported here, this can indicate the transition of a TR to a 2e-h-WMC. However, since in a QW, higher charge ECs were not observed, we can suppose that, in QWs, Coulomb interaction prevents formation

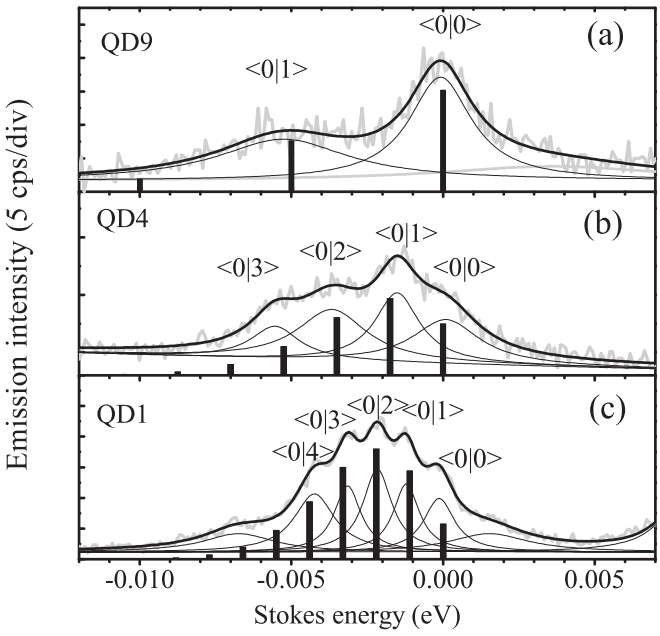

FIG. 3. Emission spectra (thick curves) of QD9, QD4, and QD1 InP/GaInP QD having values of confinement frequency $2\hbar\omega_0 =$ 4, 1.8, and 1.2 meV and $\langle 0|0\rangle$ energy 1.7236, 1.7559, and 1.7426 eV, respectively. Thin curves are Lorentzian constituents obtained from multicontour decomposition; bars are Frank-Condon factors F_N (see text).

of electron droplets, which means that some sort of Wigner crystal is formed in a weak disorder potential. Below, we report our observation of the 2e-h WMC at $B = 0$.

V. MOLECULAR COMPLEX OF SINGLE ELECTRON

A. "Vibronic" structure and TR decomposition

In Figs. 3(a)–3(c), we present NF PL Stokes energy spectra of dots QD9, QD4, and QD1, which do not have anti-Stokes components and are presumed to have only one electron. It is seen in Figs. 3(a)–3(c) that, in these dots, a Stokes structure appears and the number of Stokes components, given by N, the distribution of their intensities, and their half-widths strongly depend on $\hbar\omega_0$, similar to the situation for 2e-QDs, but here, according to Eq. (1), the separation between components is $2\hbar\omega_0$. From the spectra and their Lorentzian contour decomposition, it is seen that, for QD9 having $\hbar\omega_0 = 2$ meV($r_s = 2.7$), only the $\langle 0|1\rangle$ peak is observed, and its intensity is nearly half that of the $\langle 0|0\rangle$ peak. For QD4, having nearly half the confinement ($\hbar\omega_0 = 0.9$ meV,$r_s = 3.8$), two more components are observed (i.e. $N = 3$), and here, the $\langle 0|1\rangle$ peak becomes dominant. Further for QD1, having nearly one quarter the confinement ($\hbar\omega_0 = 0.6$ meV,$r_s = 4.7$), N increases to five, and the $\langle 0|2\rangle$ peak becomes dominant. The observed increase of N with decrease of ω_0 is accompanied by a decrease of half-width of the $\langle 0|N\rangle$ peaks from ~3 meV (QD9) to ~1.5 meV (QD1).

The intensity distributions of the $\langle 0|N\rangle$ peaks for these dots suggests a configuration in which electrons are separated in the photoexcited state, i.e. *dissociation of the TR and formation of a 2e-h WMC*. Thus, after photon emission, a residual electron remains shifted from the dot center by half a molecular bond length d_0. This generates $\langle 0|N\rangle$ components analogous to stretching vibrations in diatomic molecules [36]. Thus, the intensity distribution of Stokes components can be estimated using Frank-Condon factors $F_N = \exp(-O)^* O^N/N!$, where $O = m_e{}^*\omega_0^2(d_0/2)^2/2\hbar\omega_0$ is a Stokes shift; this is a one-dimensional approximation of 2D radial FD wave functions. We fitted F_N values for the Stokes series in Figs. 3(a)–3(c) (see corresponding bars) and obtained very good agreement with the experiment. The O values obtained are $O = 0.5$, 1.5, and 2.5, which correspond to $d_0 = 40$, 110, and 140 nm for 2e-h WMC in QD9, QD4, and QD1, respectively. For QD4, the value of d_0 is equal, first, to the size of the emission area measured using NF scanning experiments D_{NF} (see Fig. 5 and Table I in Appendix) and, second, to a diameter D of the confined electron density calculated using a configuration interaction method for a 2e-WM having $r_s = 3.8$. This value is nearly two times larger than the calculated d_0 value (see Fig. 6 in Appendix). This fact is quite surprising and needs further investigation. Since, in the case of a 2e-h WMC, the NF emission intensity maximum shifts an amount equal to d_0 from the dot center, i.e. maximum of CD distribution, we suggest that this can indicate that the states are localized at the dot edge, a situation similar to WGMs of photons in microdisk resonators [37]. The existence of such modes for an electron gas was recently demonstrated for molecules of conducting oligothiophene nanorings [38] and for a graphene gate-tunable circular cavity [39]. The existence of the states localized at the dot edge was also observed for other dots (see Fig. 5 in Appendix).

B. Vibronic structure in magnetic field

Magneto-PL data for QD1 are shown in Figs. 4(a)–4(c). In Fig. 4(a), we present NF PL spectra as a function of magnetic field strength from 0 to 10 T with a 1 T step, together with their Lorentzian contour decomposition. In Fig. 4(b), we plot

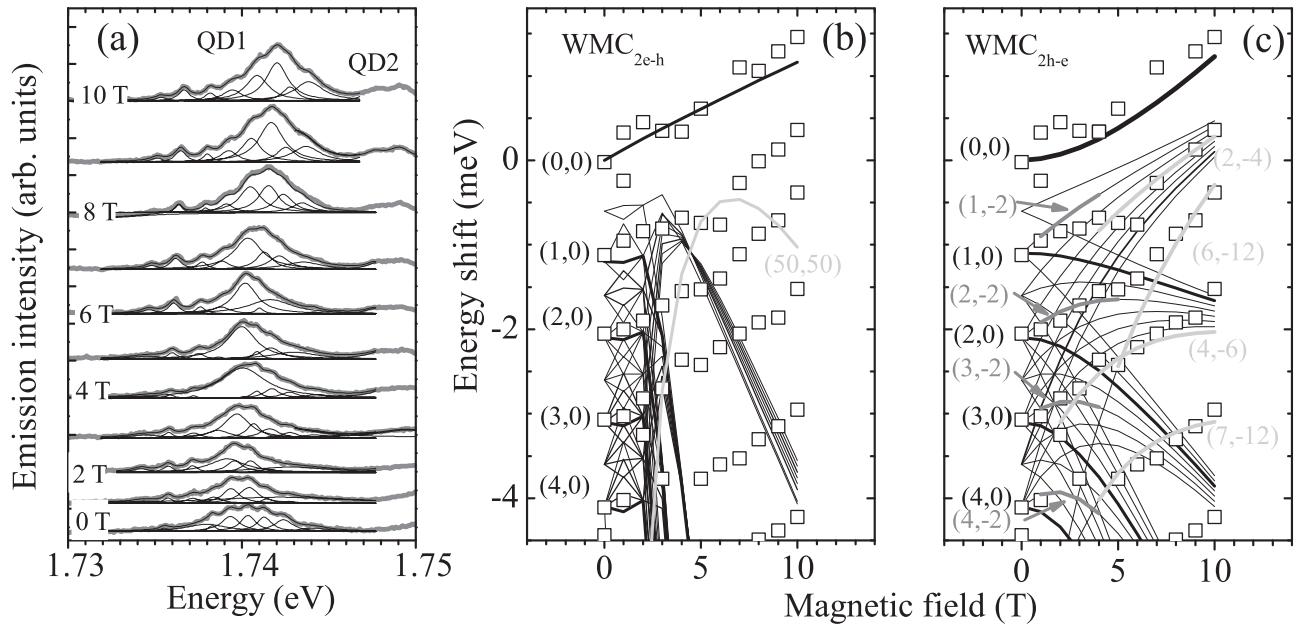

FIG. 4. (a) NF PL spectra of QD1 at magnetic field $B = 0,1,2,\ldots,10$ T, and position of the peaks versus magnetic field given by squares in (b) and (c). Calculations of the $E_{\langle 0|N\rangle}(B)$ functions (curves, see text) for a (b) 2e-h and (c) 2h-e WMC. The thin light gray curves in (b) and (c) are a set of FD states (see text). Specific FD states outlined in (b) and (c) are the $(N,0)$states = thick black curves; $(N,-2)$ = thick gray curves in (c); (50,50) = thick light gray curves in (b) and (2,−4), (6,−12), (4,−6), and (7,−12) = thick light gray curves in (c).

the shift of the emission components versus magnetic field strength.

In Fig. 4(a), the $\langle 0|N\rangle$ structure shows positive (diamagnetic) shifts with magnetic field increase. The shift of the $\langle 0|0\rangle$ peak $E_{\langle 0|0\rangle}(B)$ has value ~1.4 meV for $B = 10$ T, and nearly the same shift is observed for all $E_{\langle 0|N\rangle}(B)$ [see Fig. 4(b)].

In a parabolic potential, the emission energy of the ground state of a 2e-h WMC can be written approximately as

$$E^{\mathrm{WMC}}(B) = {E_0}^{\mathrm{WMC}}(0) + E_{C,2e}(B) + E_{\mathrm{r.m.},2e}(B) + \hbar\omega_{0h}(B). \tag{3}$$

Here, the first term is a "free" WM energy, the second term is the energy of the Coulomb interaction between electrons, the third term is the energy of relative motion of the two electrons, and the fourth term is a FD shift of the hole. In the expression in Eq. (3), we use the fact that FD levels of the c.m. motion do not depend on the number of electrons [33], i.e. $E_{\mathrm{c.m.},2e}(B) = \hbar\omega_0(B) + \mathrm{const}$. We also use the fact that ${m_h}^* \gg {m_e}^*$, and we neglect the energy of relative e-h motion. We further assume for simplicity that the energy of an e-h interaction does not depend on B. The second term in Eq. (3) represents the difference between the energy of the (0,0) state of interacting and noninteracting electrons, and it is approximately given by $E_{C,2e}(B) = 0.1\frac{\omega_c}{\sqrt{m*}}/(\sqrt[4]{\omega_c^2 + 4\omega_0^2})$ (see Ref. [40]). The third term provides spin and angular momentum transitions of the 2e ground state [41]. These include a sequence of ground states having $m = 0,-1,-2,-3,\ldots$ accompanied by spin-singlet/spin-triplet oscillations. According to the calculations of Ref. [41], the spin-singlet/spin-triplet oscillations for $r_s = 4.7$ and zero electron g factor have period ~0.7 T. The energy scale of these oscillations is, however, much smaller than the other contributions, i.e. $< 0.1E_{C,2e}(B)$ (see Ref. [22]), and thus, $E_{\langle 0|0\rangle}(B) = E^{\mathrm{WMC}}(B) - E_0^{\mathrm{WMC}}(0) \approx E_{\langle 0|0\rangle}(B)^* = E_{C,2e}(B) + \hbar\omega_{0h}(B)$. The calculated $E_{\langle 0|0\rangle}(B)^*$ reproduces well the experimentally observed shift, and the data show small oscillations around the calculated curve, which can be related to the $E_{\mathrm{r.m.},2e}(B)$ term.

For Stokes components, the term $E_{\langle 0|N\rangle}(B)$ can be written as

$$E_{\langle 0|N\rangle}(B) = E_{\langle 0|0\rangle}(B) - \theta(N+1)\hbar\omega_0(B)(2N + |M| + 1). \tag{4}$$

Here, $\theta(N+1)$ is a unit step function. Thus, it is described by single electron FD levels only, which means that it is possible to measure them experimentally and to probe the angular momentum transitions. The results of the calculations of $E_{\langle 0|N\rangle}(B)$ of a set FD states (N,M) for $N \leqslant 4, M \leqslant 8$ (see, for example, Ref. [33]) are presented in Fig. 4(b). The calculations show a strong crossing of the levels for $B < 2$ T, and their grouping around Landau levels (LLs) at higher fields. Landau levels have negative slope rapidly increasing with their number according to Eq. (4). Thus, while for $B < 2$, calculated $2N$ states follow experiment, at higher fields, the discrepancy is very strong. For high fields, only the second LL states having very high angular momentum $M \geq 20$ can provide a diamagnetic shift for the first Stokes component, as can be seen from the level (50,50) shown in Fig. 4(b), and no other states can provide such a shift for higher Stokes components. This can serve as an indication that atomiclike FD states do not correctly describe the behavior of a confined electron in a magnetic field in the weak quantum confinement at high magnetic field, possibly due to the contribution of WGMs discussed above or electron pairing discussed below.

Another possibility can be an accumulation of hole in QD1 instead of electron, and formation of a positively charged 2h-e WMC. The results of calculations of $E_{\langle 0|N\rangle}(B)$ for a 2h-e WMC, using the same assumptions as for a 2e-h WM one [42], are shown in Fig. 4(c). One can see from Fig. 4(c) that the experimental data follow $(N,-2)$ levels, indicating the $m = -2, S = 0$ state of photoexcited 2h-e-molecule in the range of $B = 1$–4. For higher fields, different Stokes components follow first LLs having higher angular momentum -4, -6, and -12 values. Thus, at $B = 4$ T, some transition occurs in 2h-e WMC. We should point out that peak assignments in Fig. 4 based on the Eq. (4) are preliminary and rather demonstrate a general evolution of Stokes peaks of 2e-h and 2h-e WMC on magnetic field based on FD states. For more precise assignment, more experimental and theoretical work is needed, which is in progress.

In a 2h-e WMC, d_0 in QD1, as estimated from the value of O, is reduced to 50 nm while r_s increases up to 13. This means that the dot is actually in the strong WL regime. Thus, for the hole, the size of NF image D_{NF} shrinks by nearly three times, which allows one to distinguish between electron and hole accumulation. From this, it follows that QD4 has a residual electron, since it has twice the confinement, and $D_{\mathrm{NF}} = 100$ nm.

The existence of a positively charged 2h-e WMC in our n-type QD sample is quite unexpected. We can suppose that appearance of this complex, implying a QD containing single residual hole, arises from very small residual acceptor doping, which can locally dominate donor doping due to statistical fluctuations.

Comparing the Wigner-Seitz radii that we have measured for the dots studied in this paper, and accounting for the fact that a TE was observed only for QD2 at zero magnetic field, we can conclude that charged exciton complexes are unstable at the onset of WL at $r_s \sim 2.5$ and seem not to exist as free quasiparticles.

VI. CONCLUSIONS

In conclusion, we used high-spatial-resolution low-temperature NF scanning optical microscopy in magnetic fields up to $B = 10$ T, and we used a weakly confined system utilizing large (~150 nm) self-organized InP/GaInP QDs, to study the stability of charged excitonic complexes and the formation of WM states, observed under these conditions. Using NF PL spectroscopy and imaging together with configuration interaction calculations, we identified dots having different electron population, quantum confinement, and size. Using dots having two electrons, we demonstrated the formation of WMs induced by magnetic field and weak quantum confinement. In dots having a single electron (hole), we demonstrated decomposition of TR and formation WMCs. Our results show that charged exciton complexes are unstable at the onset of WL. We demonstrated the use of NF PL imaging to probe the CD distribution and observed anomalous dependence of the image size on the quantum confinement,

implying formation of a WGM or clustering (pairing) of electrons in QD. We demonstrated that InP/GaInP QDs represent an excellent system for studying the effects of strong Coulomb interaction in weak quantum confined systems containing just a few electrons and holes.

ACKNOWLEDGMENTS

A.M.M. acknowledges support of the Ministry of Education and Science of the Russian Federation (Contract No. 14.Z50.31.0021, 7th April 2014).

APPENDIX: NF IMAGING AND WL

1. Size of emission area versus quantum confinement

In Figs. 5(a)–5(f), we present emission spectra and spatial distribution of emission intensity for six dots, denoted QD20, QD5, QD7, QD6, QD21, and QD4. Upper insert shows a plan-view TEM image of our QD structure having size $\sim 2000 \times 500\,\mathrm{nm}^2$. In Table I, we present electron occupation (N), quantum confinement ($\hbar\omega_0$), and the size of the emission area (D_{NF}) measured from data in Fig. 5. The table also contains the calculated size of the electron density maximum for these dots (see Fig. 6 below).

Three dots are seen in the TEM image; the dots have size $D_{\parallel}/D_{\perp} \sim 180/200$, 100/100, 170/180 nm. Two large dots show distortion of circular symmetry discussed above.

In the spectra in Figs. 5(a)–5(f), the number of the shell peaks changes from four for QD20 [Fig. 5(a)] to one for QD4 [Fig. 5(f)], and the shell splitting changes from 6–8 meV for QD20, QD5, and QD6 to 0.9–2.5 meV for QD4, QD7, and QD21.

The size of the emission area (see Table I) changes from 140–120 nm for QD7 and QD6 to 70 nm for QD20. Images of QD20, QD7, and QD4 show asymmetry, whereas images for QD5 and QD6 show symmetry. For QD21, the NF image reveals a strong maximum near the bottom and two weaker maxima near the top. These maxima are marked by white circles forming a triangle having side ~90 nm, thus resembling the maxima of the CD of three electrons (see below). The emission spectrum observed for this dot is similar to the spectra of the 2e-dot in Fig. 2, with the only exception that, here, the Stokes peaks are weaker and the $6\omega_0$ component is observed instead of $5\omega_0$, which can indicate selection rules specific to 3e WM.

TABLE I. Electron population, quantum confinement, and size of emission area[a] of InP/GaInP QDs measured using NSOM.

No.	Dot number	N	$\hbar\omega_0$ (meV)	D_{NF} (nm)	D_{CD} (nm) [b]
1	QD20	10–15	6.0	70/50	50/30
2	QD5	6–9	6.0	80	60
3	QD7	8–9[c]	1.2	140/50	140/100
4	QD6	4	8.0	120	30
5	QD21	3	2.5	90[d]	40
6	QD4	1	0.9	100/80	60/30[e]

[a]Measured as at the level of 90% of the maximum intensity (see Ref. [43]).
[b]Size of electron density maximum estimated from Fig. 6.
[c]Assuming removal of shell degeneracy.
[d]Distance between maxima, i.e. side of triangle.
[e]Assuming a 2e molecule in excited state.

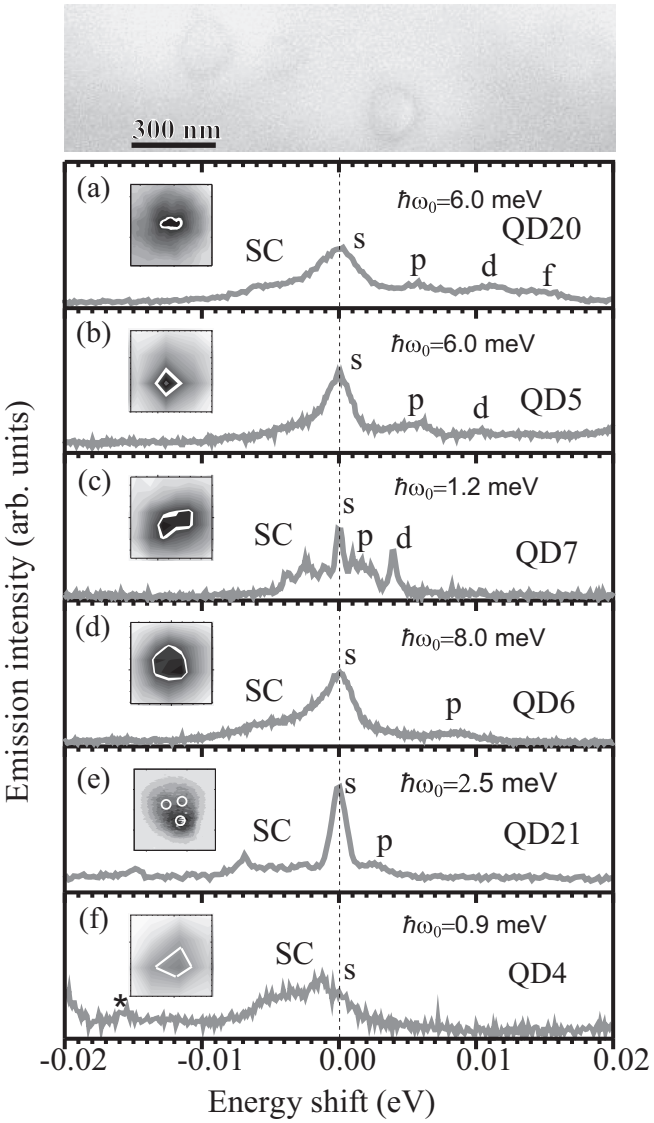

FIG. 5. NF spectra and emission intensity images (inserts) of six single InP/GaInP QDs. Emission energy of the s peak in (a)–(f) is 1.6577, 1.7299, 1.7421, 1.6942, 1.6783, and 1.7581 eV, respectively. Image size is $300 \times 300\,\mathrm{nm}^2$. White contours in images (a)–(d) and (f) outline 90% of the intensity level, and white circles in image (e) mark the position of intensity peaks. Upper insert shows $\sim 2000 \times 500\,\mathrm{nm}^2$ plan-view TEM image of structure studied.

As expected, the image size of the dots QD4, QD7, and QD21, having small confinement, is twice as large as the image size of the dots QD20 and QD5, having large confinement, but the large D_{NF} value for QD6 having $\hbar\omega_0 = 8$ meV, which is nearly equal to the D_{NF} of QD7 having $\hbar\omega_0 = 1.2$ meV, is abnormal. This can indicate some unknown effects of electron-electron interaction, such as electron pairing or formation of edge WGMs (as was discussed above). Below, we compare measured images with calculated CD distributions.

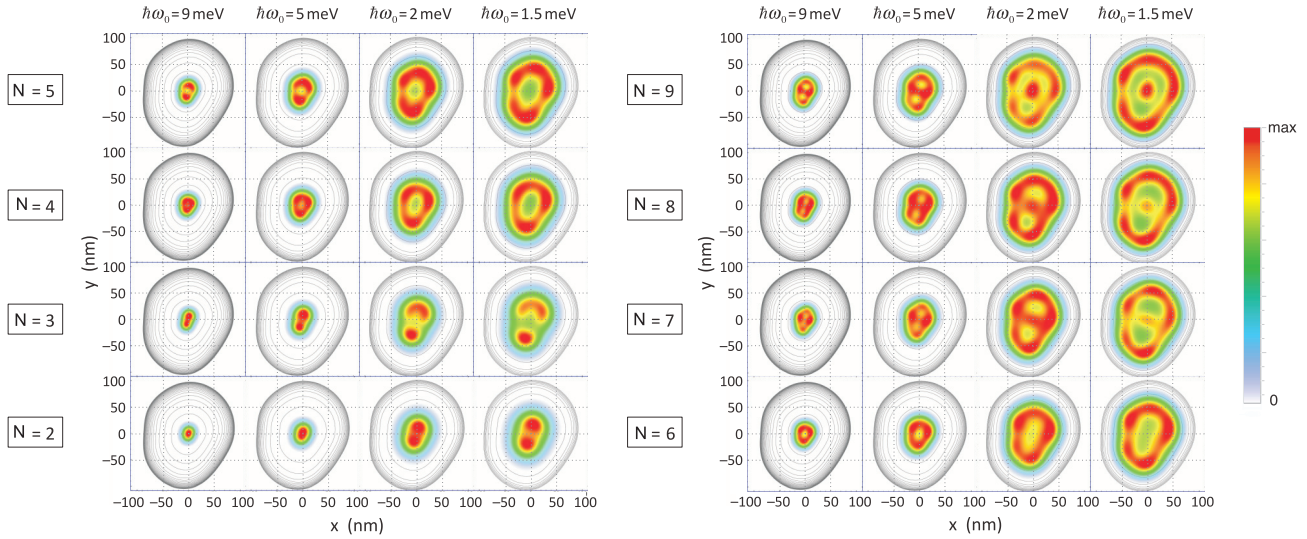

FIG. 6. CD of the ground state of N = 2–9 confined electrons. The contours indicate the confining potential, which is slightly deformed with a parabolic frequency ω_0 near the center (see text for further details).

2. Calculation of electron density distribution

Calculations of the ground-state CD for N confined electrons are shown in Fig. 6. These calculations assume a quasi-2D approximation for the electronic wave function. The effective 2D confining potential is taken to be parabolic near the center of the dot and to rise abruptly (giving a hard wall) near the physical boundary of the dot. The configuration-interaction method uses a numerical mean-field basis set suitable for weak-confinement conditions (for further details, see Ref. [26] and references therein). We took the parabolic confinement frequency ω_0 to be an adjustable parameter, considering $\hbar\omega_0 = 9.0(r_s \approx 1.0), 5.0(r_s \approx 1.5)$, $2.0(r_s \approx 2.7)$, and 1.5 meV$(r_s \approx 3.3)$. For InP QDs, the effective mass is $m_e^* = 0.08$ [44], dielectric constant is $\varepsilon = 12.61, a_B^* = 8.7$ nm, and 1 Ha* = 13.69 meV [18,19].

In Fig. 6, the lateral size of the confined electron CD naturally grows as the number N of electrons increases or as the confinement becomes weaker. The electrons are confined in most cases by the parabolic part of the potential; only for N = 7–9 and $\hbar\omega_0 \leqslant 2$ meV does the electron density approach the hard wall of the confining potential. Now, according to a fundamental theorem for the 2D electron gas [45], in a circular confining potential, the CD of a state of definite total orbital angular momentum L_z is also circularly symmetric. The CD in a circular parabolic potential then typically consists of concentric rings. A ring structure is indeed apparent in Fig. 6, but in this case, the small deformation in the confining potential breaks the circular symmetry and leads to the development of an angular structure in the rings.

Consider first the case of strong confinement, $\hbar\omega_0 \geqslant 5$ meV$(r_s \leqslant 1.5)$. Here, the electronic structure is liquidlike (or atomic) in nature and is characterized by a clearly defined shell structure, similar to that of the 2D simple harmonic oscillator. However, the states in each shell in Fig. 6 do not have definite orbital angular momenta since the deformation breaks the circular symmetry, although the deformation is small and the angular momentum is still quite well defined. Thus, the lowest energy (and radially innermost) shell (for the lowest energy, N = 1 or 2 electrons) has a predominantly s-wave character, the next shell (for N = 3–6) is predominantly p wave, and the third shell (for N = 7–10) is predominantly d wave. For example, test calculations at Hartree-Fock level indicate that the lowest-energy shell for the confinement potential of Fig. 6 has an s-wave component of 95% or higher, depending on N. (In non-closed-shell systems, many-body effects also make a small contribution to the admixture of different angular momenta.) The angular structure of the CD rings in Fig. 6 for strong confinement then arises from an interplay between the exact shape of the deformation and the predominant angular momentum of the shell in question. This produces a CD structure that at first sight seems molecular in nature but is in fact not a true WM, but rather a manifestation of the strong shell structure present at high electron densities in combination with the deformed potential.

Turning to weaker confinement, $\hbar\omega_0 \leqslant 2$ meV$(r_s \geqslant 2.5)$, we see the development of further peaks in the density rings. Thus, two peaks become visible for N = 2, three for N = 3, and five for N = 5. For most other N, there is also an increase in the number of peaks visible in the outer ring compared to the corresponding structure observed in strong confinement. We observe the same trend in calculations (not shown) of the pair correlation functions (see also Ref. [46]). This is evidence for the emergence of WL, here appearing directly in the CD, for $r_s \geqslant 2.5$. In calculations at much higher $r_s = 8$ (not shown), we find a clearly resolved localization of individual electrons with the following geometries: equilateral triangle (N = 3), square (N = 4), pentagon (N = 5), pentagon with one electron in the center (N = 6), hexagon with one electron in the center (N = 7), heptagon with one electron in the center (N = 8), and deformed heptagon with two electrons in the center (N = 9). (Note that, at intermediate $r_s \sim 3$, the geometry of N = 6 is hexagonal, which can be observed in Fig. 6, but at higher r_s, a transition to a pentagonal symmetry occurs).

The small deformation and hard-wall potential leads to stronger localization, which results in increased "valley depth" between the outer shell and the central motif. In Fig. 6, for $N = 7$, it is two times deeper compared to a circular dot (40 versus 20%; see Ref. [47]) indicating large effective r_s. Also, a modulation of the CD in the outer ring by up to 20% resolves the localization of individual electrons. Thus, the recombination of the photoexcited hole with the partially localized electrons gives the shell structure (including the shell occupied by photoexcited electron) observed experimentally in the emission spectrum.

We found a reasonable agreement between the size of the charged densities and NF image size for QD7 and QD5, having small and large confinement, respectively.

For QD21, the shape of the NF image is close to the CD shape for $N = 3$ and $\hbar\omega_0 = 2$ meV, but the calculated triangle side (40 nm) is two times smaller. For QD6, we suggest $N = 4$, which has a more symmetric CD distribution. For this dot, $D_{CD}(\sim 50\,\text{nm})$ is two times smaller than D_{NF} as well. Large D_{NF} observed for these dots can indicate larger N, which, however, implies a clustering (for example, pairing) of the electrons in the QD. These issues need further investigations.

[1] Ye. F. Gross and N. A. Karryev, Dokl. Akad. Nauk SSSR **84**, 261 (1952).

[2] N. F. Mott, Proc. R. Soc. London, Ser. A **167**, 384 (1938); G. H. Wannier, Phys. Rev. **52**, 191 (1937).

[3] M. A. Lampert, Phys. Rev. Lett. **1**, 450 (1958).

[4] M. Ediger, G. Bester, A. Badolato, P. M. Petroff, K. Karrai, A. Zunger, and R. J. Warburton, Nat. Phys. **3**, 774 (2007).

[5] K. Kheng, R. T. Cox, Y. M. d'Aubigne, F. Bassani, K. Saminadayar, and S. Tatarenko, Phys. Rev. Lett. **71**, 1752 (1993).

[6] G. Finkelstein, H. Shtrikman, and I. Bar-Joseph, Phys. Rev. Lett. **74**, 976 (1995).

[7] A. J. Shields, M. Pepper, M. Y. Simmons, and D. A. Ritchie, Phys. Rev. B **52**, 7841 (1995).

[8] A. J. Shields, J. L. Osborne, M. Y. Simmons, M. Pepper, and D. A. Ritchie, Phys. Rev. B **52**, R5523 (1995).

[9] G. Finkelstein, H. Shtrikman, and I. Bar-Joseph, Phys. Rev. B **53**, R1709 (1996).

[10] A. Haury, A. Arnoult, V. A. Chitta, J. Cibert, Y. Merle d'Aubige, S. Tatarenko, and A. Wasiela, Superlattices Microstruct. **23**, 1097 (1998).

[11] G. Eytan, Y. Yayon, M. Rappaport, H. Shtrikman, and I. Bar-Joseph, Phys. Rev. Lett. **81**, 1666 (1998).

[12] V. V. Solovyev and I. V. Kukushkin, Phys. Rev. B **79**, 233306 (2009).

[13] G. V. Astakhov, D. R. Yakovlev, V. P. Kochereshko, W. Ossau, W. Faschinger, J. Puls, F. Henneberger, S. A. Crooker, Q. McCulloch, and D. Wolverson, Phys. Rev. B **65**, 165335 (2002).

[14] A. S. Bracker, E. A. Stinaff, D. Gammon, M. E. Ware, J. G. Tischler, D. Park, D. Gershoni, A. V. Filinov, M. Bonitz, F. Peeters, and C. Riva, Phys. Rev. B **72**, 035332 (2005).

[15] C. Schulhauser, D. Haft, R. J. Warburton, K. Karrai, A. O. Govorov, A. V. Kalameitsev, A. Chaplik, W. Schoenfeld, J. M. Garcia, and P. M. Petroff, Phys. Rev. B **66**, 193303 (2002).

[16] A. O. Govorov, C. Schulhauser, D. Haft, A. V. Kalameitsev, A. Chaplik, R. J. Warburton, K. Karrai, W. Schoenfeld, J. M. Garcia, and P. M. Petroff, arXiv:cond-mat/0202480 (2002).

[17] E. P. Wigner, Phys. Rev. **46**, 1002 (1934).

[18] In effective atomic units $a_B^* = \hbar^2(4\pi\varepsilon\varepsilon_0)/m^*e^2$, where ϵ and m^* are dielectric constant of the material and effective mass of electron, respectively.

[19] In effective atomic units $\text{Ha}^* = 2\text{Ry}^*$, where Rydberg, $\text{Ry}^* = m^*e^4/2\hbar^2(4\pi\varepsilon\varepsilon_0)^2$.

[20] B Szafran, S. Bednarek, and J. Adamowski, J. Phys.: Condens. Matter **15**, 4189 (2003).

[21] U. Merkt, J. Huser, and M. Wagner, Phys. Rev. B **43**, 7320 (1991).

[22] D. Pfanncuche, R. R. Gerhardts, P. A. Maksym, and V. Gudmundsson, Physica B **189**, 6 (1993).

[23] C. Yannouleas and U. Landman, Phys. Rev. Lett. **85**, 1726 (2000).

[24] S. Kalliakos, C. P. García, V. Pellegrini, M. Zamfirescu, L. Cavigli, M. Gurioli, A. Vinattieri, A. Pinczuk, B. S. Dennis, L. N. Pfeiffer, and K. W. West, Appl. Phys. Lett. **90**, 181902 (2007).

[25] S. Kalliakos, M. Rotani, V. Pellegrini, C. P. García, A. Pinczuk, G. Goldoni, E. Molinari, L. N. Pfeiffer, and K. W. West, Nat. Phys. **4**, 467 (2008).

[26] J. Kapaldo, S. Rouvimov, J. L. Merz, S. Oktyabrsky, S. A. Blundell, N. Bert, P. Brunkov, N. A. Kalyuzhnyy, S. A. Mintairov, S. Nekrasov, R. Saly, A. S. Vlasov, and A. M. Mintairov, J. Phys. D: Appl. Phys. **49**, 475301 (2016).

[27] A. M. Mintairov, J. L. Merz, and S. Blundell, *Fingerprints in the Optical and Transport Properties of Quantum Dots* (InTech, 2012), pp. 125–152.

[28] A. Wojs and P. Hawrylak, Phys. Rev. B **55**, 13066 (1997).

[29] J. Y. Fu, S. D. Lin, M. F. Tsai, H. Lin, C. H. Lin, C. H. Chou, S. J. Cheng, and W. H. Chang, Phys. Rev. B **81**, 113307 (2010).

[30] S. Cao, J. Tang, Y. Sun, K. Peng, Y. Gao, Y. Zhao, C. Qian, S. Sun, H. Ali, Y. Shao, S. Wu, F. Song, D. A. Williams, W. Sheng, K. Jin, and X. Xu, Nano Res. **9**, 306 (2016).

[31] E. Margapoti, F. M. Alves, S. Mahapatra, V. Lopez-Richard, L. Worschech, K. Brunner, F. Qu, C. Destefani, E. Menéndez-Proupin, C. Bougero, A. Forchel, and G. E. Marques, New J. Phys. **14**, 043038 (2012).

[32] L. Bouet, M. Vidal, T. Mano, N. Ha, T. Kuroda, M. V. Durnev, M. M. Glazov, E. L. Ivchenko, X. Marie, T. Amand, K. Sakoda, G. Wang, and B. Urbaszek, Appl. Phys. Lett. **105**, 082111 (2014).

[33] L. Jacak, P. Hawrylak, and A. Wojs, *Quantum Dots* (Springer, Berlin, 1998), p. 176.

[34] J. Leotin, R. Barbaste, S. Askenazy, M. S. Skolnick, R. A. Stradling, and J. Tuchendler, Solid State Commun. **15**, 693 (1974).

[35] G. Finkelstein, H. Shtrikman, and I. Bar-Joseph, Phys. Rev. B **53**, 12593 (1996).

[36] K. K. Rebane, *Impurity Spectra of Solids: Elementary Theory of Vibrational Structure* (Springer US, Plenum Press, New York, 1970), p. 253.

[37] A. M. Mintairov, Y. Chu, Y. He, S. Blokhin, A. Nadtochy, M. Maximov, V. Tokranov, S. Oktyabrsky, and J. L. Merz, Phys. Rev. B **77**, 195322 (2008).

[38] G. Reecht, H. Bulou, F. Scheurer, V. Speisser, B. Carriere, F. Mathevet, and G. Schull, Phys. Rev. Lett. **110**, 056802 (2013).

[39] Y. Zhao, J. Wyrick, F. D. Natterer, J. F. Rodriguez-Nieva, Cyprian Lewandowski, K. Watanabe, T. Taniguchi, L. S. Levitov, N. B. Zhitenev, and J. A. Stroscio, Science **348**, 672 (2015).

[40] J. Kyriakidis, M. Pioro-Ladriere, M. Ciorga, A. S. Sachrajda, and P. Hawrylak, Phys. Rev. B **66**, 035320 (2002).

[41] M. Wagner, U. Merkt, and A. V. Chaplik, Phys. Rev. B **45**, 1951(R) (1992).

[42] For 2h-e WMC, we used electron effective mass $0.24m_0^*$ to fit $E_{\langle 0|0\rangle}(B)$ shift, and three times increase of electron effective mass probably accounts for e-h interaction neglected in the expression in Eq. (3).

[43] A. M. Mintairov, J. Kapaldo, J. L. Merz, S. Rouvimov, N. Kalyygniy, S. A. Mintairov, S. Nekrasov, R. Saly, A. S. Vlasov, and S. Blundell, AIP Conf. Proc. **1748**, 020001 (2016).

[44] C. Pryor, M.-E. Pistol, and L. Samuelson, Phys. Rev. B **56**, 10404 (1997).

[45] K. Hirose and N. S. Wingreen, Phys. Rev. B **59**, 4604 (1999).

[46] A. Ghosal, A. D. Güçlü, C. J. Umrigar, D. Ullmo, and H. U. Baranger, Nat. Phys. **2**, 336 (2006).

[47] A. Ghosal, A. D. Güçlü, C. J. Umrigar, D. Ullmo, and H. U. Baranger, Phys. Rev. B **76**, 085341 (2007).